BVRI Photometry of SN 2016coj in NGC 4125

Michael Richmond
School of Physics and Astronomy, Rochester Institute of Technology, Rochester, NY 14623, mwrsps@rit.edu

Brad Vietje
Northeast Kingdom Astronomy Foundation, PO Box 173, Peacham, VT 05862, brad@nkaf.org

Received April 12, 2017; revised June 6, 2017; accepted June 6, 2017

Abstract We present BVRI photometry of supernova (SN) 2016coj in NGC 4125 from 9 days before to 57 days after its *B*-band maximum light. Our light curves and color curves suggest that this event belongs to the "normal" class of type Ia SNe, with a decline rate parameter $\Delta m_{15}(B) = 1.32 \pm 0.10$, and that it suffers little extinction. Adopting a distance modulus to its host galaxy of $(m - M) = 31.89$ mag, we compute extinction-corrected peak absolute magnitudes of $M_B = -19.01$, $M_V = -19.05$, $M_R = -19.03$, and $M_I = -18.79$. The explosion occurred close enough to the nucleus of NGC 4125 to hinder the measurement of its brightness. We describe our methods to reduce the effect of such host-galaxy contamination, but it is clear that our latest values suffer from systematic bias.

1. Introduction

Supernova (SNe) of type Ia are thought to originate in close binary systems, consisting of either a single white dwarf and a main-sequence companion, or two white dwarfs. When one white dwarf accretes enough material to exceed the Chandrasekhar limit (Chandrasekhar 1931), either by long-term transfer from a main sequence companion, or by a violent merger with another white dwarf, a runaway thermonuclear reaction propagates through it, disrupting the entire white dwarf, heating the ejecta to hundreds of thousands of degrees and blowing it out into space at thousands of kilometers per second. The expanding cloud of hot gas radiates energy for several months, reaching absolute magnitudes in the optical of order –18 to –20. Many (but not all) type Ia SNe exhibit similar properties, with a correlation between the shape of the light curve and the absolute magnitude at peak (Phillips 1993). When events are observed in sufficient detail, one can use the shape of the light curve to compute the absolute magnitude (Prieto *et al.* 2006; Guy *et al.* 2005), and so use these SNe as "standard-izable candles" to determine distances.

Supernova 2016coj in the galaxy NGC 4125, a peculiar elliptical of class E6 (de Vaucouleurs *et al.* 1991), was discovered by the Lick Observatory Supernova Search (Filippenko *et al.* 2001; Leaman *et al.* 2011) on UT 2016 May 28 (Zheng *et al.* 2016) and quickly identified as a type Ia explosion. Since its host galaxy is relatively close to our Milky Way, at a redshift of only z = 0.004523 according to the NASA Extragalactic Database (NED; see https://ned.ipac.caltech.edu), this event promised to provide a wealth of high-precision information. However, since the supernova occurred not far from the galaxy's nucleus, disentangling its light from that of the surrounding stars turns out to be a difficult task.

In this paper, we describe photometry of SN 2016coj in the BVRI passbands acquired at two locations, starting on UT 2016 May 30 and ending UT 2016 Aug 4, an interval of 66 days. Section 2 describes our observational methods, the cleaning of the raw CCD images, and the techniques we used to extract instrumental magnitudes. We explain our photometric calibration of the raw measurements onto the standard Johnson-Cousins system in section 3. The light curves and color curves of the event are shown in section 4; we comment briefly on their properties and the effect of extinction along the line of sight. We present our conclusions in section 5. In an appendix, we discuss the difficulties of measuring the light of a point source immersed in a non-uniform background, and use simple simulations to estimate the nature of systematic biases that appear in our data.

2. Observations

We present herein data acquired at the RIT Observatory, near Rochester, New York, and at the Northern Skies Observatory (NSO), in Peacham, Vermont. We will describe below the procedures by which we acquired and reduced the images from each observatory in turn.

The RIT Observatory is located on the southeastern corner of the Rochester Institute of Technology campus, at longitude 77:39:53 West, latitude +43:04:33 North, and an altitude of 168 meters. Our Meade LX200 f/10 30-cm telescope provides a plate scale of 1.38" per pixel at the focus of our SBIG ST-9 camera, which has BVRI filters built to the Bessell prescription. When observing SN 2016coj, we acquired a series of 5 to 20 short exposures (exposure times 30 seconds each up to 2016 July 19 = JD 2457588, 120 seconds each after that date), discarding those with trailing or extinction by clouds. We acquired dark and flatfield images each night, creating master frames from the median of 10 individual images. Flatfields were based on images of the twilight sky, with the exception of UT June 13, when bad conditions forced us to use dome flats. After subtracting the master dark from each target frame and dividing it by the normalized master flatfield, we examined each resulting "clean" image by eye, discarding those with poor quality.

Before extracting instrumental magnitudes, we combined all the images in a particular passband using a median technique, in order to increase the signal-to-noise ratio and eliminate cosmic rays. Figure 1 shows an example of such a combined image, with labels indicating stars used for calibration.

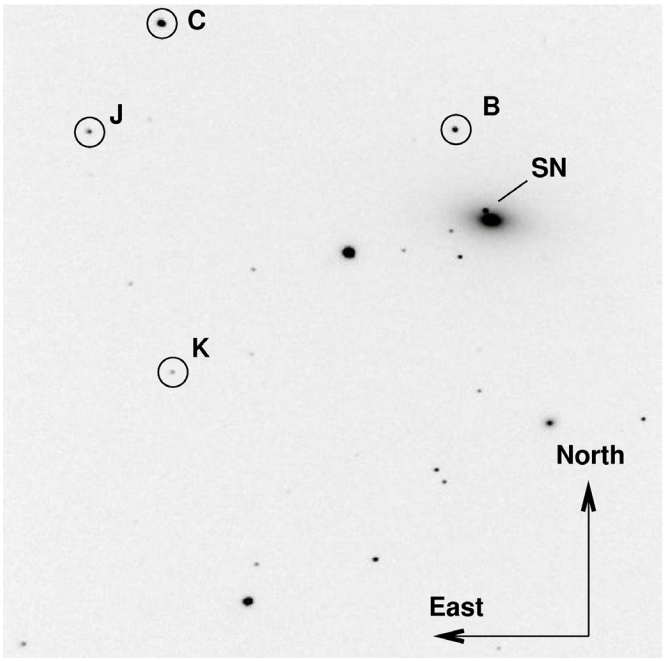

Figure 1. R-band composite (16 images of 30 seconds each) of SN 2016coj from RIT, showing stars used to calibrate measurements. North is up, East to the left. The field of view is roughly 12 by 12 arcminutes.

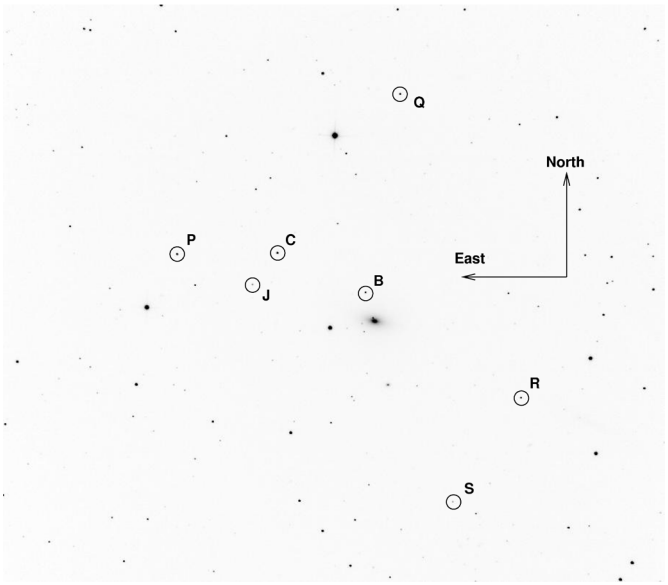

Figure 3. R-band composite (5 images of 45 seconds each) of SN 2016coj from NSO, showing stars used to calibrate measurements. North is up, East to the left. The field of view is roughly 30 by 30 arcminutes.

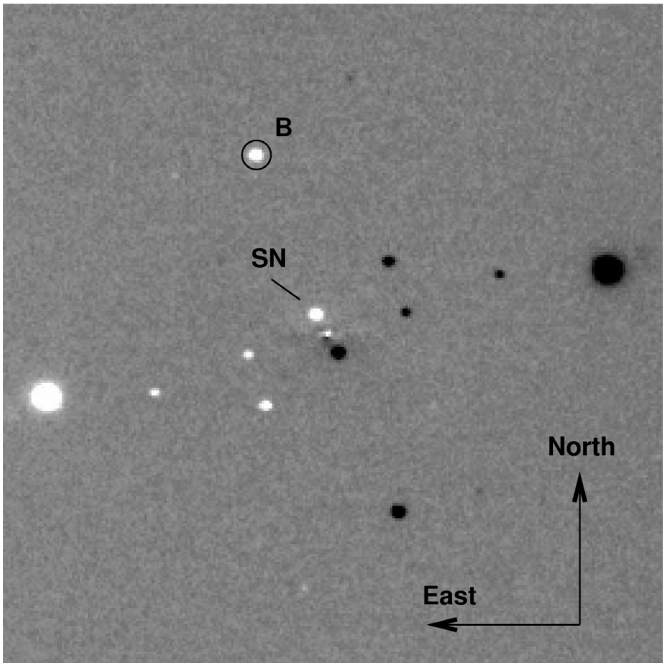

Figure 2. The residual after rotation and subtraction of an image from RIT taken UT 2016 June 24. Positive residuals are bright and negative dark. North is up, East to the left; the galaxy's nucleus appears at the center. The field of view is roughly 7 by 7 arcminutes.

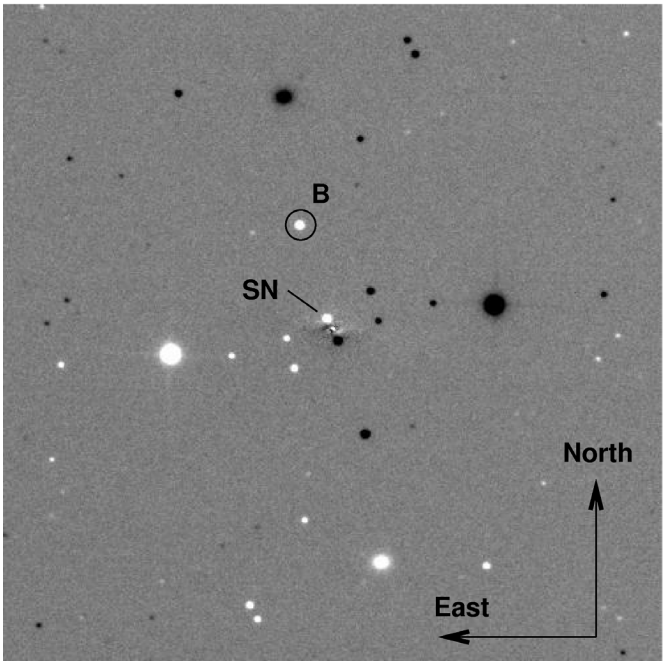

Figure 4. The residual after rotation and subtraction of an image from NSO taken UT 2016 June 26. Positive residuals are bright and negative dark. North is up, East to the left; the galaxy's nucleus appears at the center. The field of view is roughly 10 by 10 arcminutes.

Table 1. Photometry of comparison stars.

Star	*R.A. (J2000)* *h m s*	*Dec. (J2000)* ° ′ ″	*B*	*V*	*R*	*I*
B	12 08 11.72	+65 12 04.7	15.198 ± 0.086	14.133 ± 0.052	13.627 ± 0.116	13.155 ± 0.156
C	12 09 01.20	+65 14 03.5	13.317 ± 0.093	12.673 ± 0.058	12.316 ± 0.121	11.980 ± 0.161
J	12 09 13.84	+65 12 09.7	15.607 ± 0.109	14.956 ± 0.065	14.603 ± 0.136	14.271 ± 0.182
K	12 09 00.39	+65 07 51.9	16.573 ± 0.123	15.975 ± 0.082	15.547 ± 0.174	15.147 ± 0.231
P	12 09 56.10	+65 13 37.8	13.778 ± 0.095	13.113 ± 0.058	12.750 ± 0.116	12.409 ± 0.154
Q	12 08 11.72	+65 12 04.7	15.198 ± 0.086	14.133 ± 0.052	13.627 ± 0.116	13.155 ± 0.156
R	12 06 43.72	+65 06 30.3	15.392 ± 0.097	14.424 ± 0.058	13.911 ± 0.119	13.432 ± 0.158
S	12 07 17.93	+65 00 19.8	15.929 ± 0.108	15.246 ± 0.065	14.869 ± 0.128	14.515 ± 0.169

The Point Spread Function (PSF) of these combined images had a typical Full Width at Half Maximum (FWHM) of 3.5" to 4.1".

Since the supernova lies only about 12 arcseconds from the nucleus of its host galaxy (Zheng *et al.* 2016), simple aperture photometry will yield poor results. A systematic error can appear in such measurements due to imperfect background subtraction; the size of the error will grow as the supernova fades. A standard technique in such cases is to match each target image to a template of the same galaxy taken some time before or after the event, in which the supernova does not appear, and then to subtract the template from the target image. However, since we lacked template images, we adopted a technique which does not require them; the drawback is that its results are less accurate, and can still suffer from systematic effects. See the Appendix for a detailed explanation.

The basic idea of the method is to use the symmetry of the elliptical galaxy host to provide a pseudo-template. We identified the center of the host galaxy, rotated the image by 180° around this point, then subtracted the rotated version from the original. An example of the results, starting with the same image shown in Figure 1, is displayed in Figure 2; we have zoomed in to show details near the nucleus more clearly. The subtraction is not perfect: small positive and negative residuals remain near the center of the galaxy. However, the residuals decrease rapidly with radius, and near the position of the supernova they are typically much smaller than the peak of the supernova's light. Moreover, the background around and underneath the supernova is much more uniform than in the original image, removing the main source of error in the aperture photometry.

After creating these residual images, we performed standard aperture photometry of the SN and reference stars, using the XVista (Treffers and Richmond 1989) routines STARS and PHOT. We chose to measure light within circular apertures of a fixed radius, a bit larger than the usual FWHM: 4 pixels = 5.5". A local sky background was estimated for each star using an annulus with radii of 6.9" and 13.8".

The Northern Skies Observatory is located in Peacham, Vermont, at longitude 72:09:57 West, latitude +44:19:30 North, and an elevation of 384 meters above sea level. Images of SN 2016coj were acquired through a 43-cm f/6.8 corrected Dall-Kirkham astrograph made by PlaneWave Instruments. Light passes through Johnson-Cousins BVRI filters before reaching an Apogee Alta U16M CCD camera; we bin the chip 2 × 2 to produce a plate scale of 1.26" per pixel. We acquire new flatfield images for each observing session, but re-use bias and dark frames for a month or so. We acquired 5 unguided images in each passband, using exposure times of 45 to 60 seconds each. After using MAXIMDL (Diffraction Ltd. 2012) to subtract master bias and master dark frames, and divide by a master flatfield frame, we combined the images in each passband using a median technique. These combined images typically had a FWHM ranging between 3.1" and 3.9", with most lying near the low end of this range. A sample composite R-band image is shown in Figure 3.

We applied the rotation technique described above to each combined image before extracting photometry using circular apertures of radius 3 pixels = 3.8". The local background was measured for each star using an annulus of radii 12.6" and 25.2". Figure 4 shows one such residual image from the NSO dataset.

3. Photometric calibration

In order to transform our instrumental measurements onto the standard Johnson-Cousins BVRI system, we used a set of local reference stars (Table 1) provided by the American Association of Variable Star Observers (AAVSO; https://www.aavso.org) in their sequence X18345FX. These stars are labelled in all figures showing the supernova and its surroundings. Given our relatively small fields of view and shallow limiting magnitudes, we did not select comparison stars on the basis of color, but accepted them all. The color range covered is relatively small: $0.598 \leq (B–V) \leq 1.065$. SN 2016coj has a color of $(B–V) \simeq 0.0$ near maximum light, and does not redden to match the comparison stars until about 15 days later. Of course, the spectrum of this type Ia SN is so distinct from that of the comparison stars that color corrections must be approximate in any case.

In order to convert the RIT measurements to the Johnson-Cousins system, we analyzed images of the standard fields PG1633+009 and PG2213-006 (Landolt 1992) taken on five nights between June and August 2016. Comparing our instrumental values to the standard magnitudes, we determined transformation equations

$$B = b + 0.2016(0134) \times (b−v) + Z_B \quad (1)$$

$$V = v − 0.0920(0063) \times (v−r) + Z_V \quad (2)$$

$$R = r – 0.1137\ (0058) \times (r–i) + Z_R \quad (3)$$

$$I = i – 0.0174\ (0034) \times (r–i) + Z_I \quad (4)$$

Table 2. RIT photometry of SN 2016coj.

JD−2457530	B	V	R	I	Comments
9.64	14.108 ± 0.040	13.960 ± 0.029	13.811 ± 0.067	13.866 ± 0.085	
10.61	13.816 ± 0.042	13.760 ± 0.021	13.657 ± 0.020	13.677 ± 0.040	
11.61	13.663 ± 0.067	13.556 ± 0.028	13.432 ± 0.104	13.484 ± 0.125	cirrus
19.60	13.231 ± 0.062	13.072 ± 0.038	13.061 ± 0.021	13.426 ± 0.073	
20.59	13.371 ± 0.090	13.109 ± 0.057	13.070 ± 0.038	13.503 ± 0.105	cirrus
21.58	13.244 ± 0.077	13.139 ± 0.049	13.161 ± 0.040	13.548 ± 0.049	light clouds
22.64	13.368 ± 0.058	13.196 ± 0.057	13.268 ± 0.077	13.822 ± 0.136	
23.59	13.415 ± 0.027	13.179 ± 0.029	13.212 ± 0.021	13.714 ± 0.059	
24.59	13.480 ± 0.049	13.232 ± 0.029	13.369 ± 0.046	13.837 ± 0.101	cirrus
27.60	13.884 ± 0.045	13.409 ± 0.027	13.544 ± 0.061	13.970 ± 0.065	
28.60	13.998 ± 0.050	13.440 ± 0.022	13.632 ± 0.059	13.984 ± 0.063	cirrus
29.61	13.975 ± 0.096	13.472 ± 0.030	13.543 ± 0.065	13.859 ± 0.088	bright moon
31.61	14.270 ± 0.072	13.586 ± 0.028	13.648 ± 0.079	13.719 ± 0.111	
32.59	14.436 ± 0.049	13.639 ± 0.023	13.648 ± 0.072	13.750 ± 0.085	
33.60	14.535 ± 0.088	13.650 ± 0.024	13.675 ± 0.057	13.723 ± 0.087	
36.59	15.166 ± 0.222	13.865 ± 0.048	13.656 ± 0.088	13.608 ± 0.085	clouds
37.59	15.129 ± 0.091	13.964 ± 0.052	13.670 ± 0.066	13.572 ± 0.099	fewer images
39.60	15.400 ± 0.115	14.061 ± 0.030	13.737 ± 0.069	13.516 ± 0.086	
40.60	15.370 ± 0.069	14.155 ± 0.043	13.795 ± 0.061	13.418 ± 0.104	
42.60	15.678 ± 0.119	14.349 ± 0.044	13.948 ± 0.072	13.593 ± 0.086	
43.60	15.722 ± 0.078	14.421 ± 0.040	14.034 ± 0.081	13.705 ± 0.095	
45.60	15.938 ± 0.079	14.586 ± 0.044	14.248 ± 0.078	13.840 ± 0.082	haze
50.60	16.026 ± 0.117	14.822 ± 0.069	14.462 ± 0.093	14.372 ± 0.106	cirrus
51.60	15.844 ± 0.189	14.897 ± 0.049	14.578 ± 0.085	14.272 ± 0.113	cirrus
53.60	16.265 ± 0.107	14.926 ± 0.062	14.654 ± 0.081	14.414 ± 0.107	haze, old flats
56.60	16.193 ± 0.117	15.100 ± 0.055	14.799 ± 0.082	14.596 ± 0.098	
58.60	16.002 ± 0.113	15.111 ± 0.058	14.796 ± 0.086	14.609 ± 0.113	
59.60	16.202 ± 0.102	15.069 ± 0.047	14.815 ± 0.064	14.623 ± 0.084	start longer exp
62.60	—	15.188 ± 0.035	14.915 ± 0.084	14.686 ± 0.110	
63.61	—	15.222 ± 0.063	15.032 ± 0.090	14.824 ± 0.124	cirrus
65.60	—	15.257 ± 0.038	15.020 ± 0.062	14.840 ± 0.082	
66.60	—	15.289 ± 0.049	15.061 ± 0.082	14.839 ± 0.125	cirrus
69.62	—	15.374 ± 0.041	15.176 ± 0.087	14.928 ± 0.083	light clouds
72.60	—	15.433 ± 0.036	15.211 ± 0.083	14.949 ± 0.089	
73.59	—	15.451 ± 0.039	15.235 ± 0.069	15.118 ± 0.090	
75.61	—	15.503 ± 0.092	15.421 ± 0.108	15.054 ± 0.126	light clouds

In the equations above, lower-case symbols represent instrumental magnitudes, upper-case symbols Johnson-Cousins magnitudes, terms in parentheses the uncertainties in each coefficient, and Z the zeropoint in each band. The relatively small field of view of the RIT images allowed us to use only a few stars for calibration: B, C, J, and, in some cases, K.

In mid-June 2016, we noticed that images in the *B*-band from RIT had a low signal-to-noise ratio, even after coaddition; this is largely a function of the relatively low sensitivity of our camera's sensor at short wavelengths. The *B*-band measurements showed a large scatter from night to night, making real trends in the light curve hard to discern. Therefore, after UT 2016 June 20, we stopped taking images at RIT in the *B*-band.

We present our calibrated measurements of SN 2016coj made at RIT in Table 2. The first column shows the mean Julian Date of all the exposures taken during each night; we have subtracted the arbitrary constant 2457530 from all Julian Dates for convenience. The uncertainties listed in Table 2 incorporate the uncertainties in instrumental magnitudes and in the offset to shift the instrumental values to the standard scale, added in quadrature.

We determined linear transformations between the instrumental NSO measurements and the standard scale using images of the open cluster M67 and photometry provided by the AAVSO. The transformation equations for NSO were

$$B = b - 0.164(0.033) \times (b-v) + Z_B \quad (5)$$

$$V = v - 0.109(0.023) \times (b-v) + Z_V \quad (6)$$

$$V = v - 0.197(0.050) \times (v-r) + Z_V \quad (7)$$

$$R = r - 0.205(0.052) \times (r-i) + Z_R \quad (8)$$

$$I = i - 0.238(0.073) \times (r-i) + Z_I \quad (9)$$

In the equations above, lower-case symbols represent instrumental magnitudes, upper-case symbols Johnson-Cousins magnitudes, terms in parentheses the uncertainties in each coefficient, and *Z* the zeropoint in each band. We list two equations for the *V*-band; on nights when we acquired *R* images, we used the (*v*–*r*) equation, but on nights when we measured only *B* and *V*, we used the (*b*–*v*) version.

Table 3 lists our calibrated measurements of SN 2016coj made at Northern Skies Observatory.

4. Light curves

In order to determine the time and magnitude at peak brightness, we fit polynomials of order 3 to the light curves near maximum, using data from the period 0 < (JD – 2457530)

Table 3. NSO photometry of SN 2016coj.

JD–2457530	*B*	*V*	*R*	*I*
20.64	13.307 ± 0.023	13.073 ± 0.027	13.121 ± 0.037	13.570 ± 0.057
25.64	13.606 ± 0.056	13.242 ± 0.015	—	—
33.65	14.565 ± 0.038	13.791 ± 0.017	13.773 ± 0.035	13.967 ± 0.056
34.63	14.682 ± 0.025	13.845 ± 0.026	13.769 ± 0.034	13.824 ± 0.047
35.64	14.785 ± 0.058	13.807 ± 0.032	—	—
39.61	15.195 ± 0.067	14.037 ± 0.032	—	—
42.61	15.487 ± 0.034	14.369 ± 0.028	14.000 ± 0.036	13.687 ± 0.065
43.66	15.626 ± 0.047	14.461 ± 0.030	14.110 ± 0.039	13.729 ± 0.058
45.59	15.729 ± 0.043	14.632 ± 0.031	—	—
73.59	16.423 ± 0.058	15.590 ± 0.038	15.456 ± 0.042	15.535 ± 0.075

Table 4. Apparent magnitudes at maximum light.

Passband	*JD–2457530*	*Magnitude*
B	18.1 ± 0.4	13.16 ± 0.07
V	18.7 ± 0.2	13.06 ± 0.01
R	18.0 ± 0.4	13.04 ± 0.03
I	16.2 ± 2.9	13.23 ± 0.10
I (sec)	39.0 ± 0.7	13.50 ± 0.05

< 30 in each passband, weighting the fits by the uncertainties in each measurement. We list the results in Table 4. For the secondary maximum in *I*-band, we found that polynomials of order 2 provided better fits; we averaged the results from several intervals during during the period 30 < (JD – 2457530) < 50 to produce the value in the table. Note that the *I*-band magnitude at its primary maximum is particularly uncertain, as it falls farther within the gap in our measurements than the peaks in other passbands.

Using a second-order polynomial to interpolate in the B-band observations exactly 15 days after the time of B-band maximum light, we compute $\Delta_{15}(B) = 1.32 \pm 0.10$. By this measure, SN 2016coj lies in the range of "normal" type Ia SNe, such as 1980N (Hamuy *et al.* 1991), 1989B (Wells *et al.* 1994), 1994D (Richmond *et al.* 1995), 2003du (Stanishev *et al.* 2007), and 2011fe (Richmond and Smith 2012; Parrent *et al.* 2012). The secondary peak in *I*-band, which lies 22.8 ± 1.0 days after and 0.27 ± 0.07 magnitude below the primary peak, is also typical of "normal" type Ia events.

Our values of the apparent magnitude at *B*-band maximum light and the $\Delta_{15}(B)$ parameter agree with those measured by Zheng *et al.* (2016). Those authors also provide spectroscopic evidence to support a "normal" classification for SN 2016coj.

In order to compute absolute magnitudes and intrinsic colors for SN 2016coj, we must remove the extinction due to any intervening material. Fortunately, there appears to be very little dust in its direction. Our own Galaxy's contribution is small: Schlegel *et al.* (1998) use infrared maps of the Milky Way to estimate $E(B–V)_{MW} = 0.017$ in the direction of NGC 4125. Zheng *et al.* (2016) examine high-resolution spectra of SN 2016coj to look for absorption lines caused by interstellar material in the host galaxy. Finding none, they employ several methods to place upper limits on the reddening of $E(B–V)_{host} \lesssim 0.05$ or $E(B–V)_{host} \lesssim 0.09$. We will adopt a host value of $E(B–V)_{host} = 0.05$ for the color curves we present below, yielding a total reddening of $E(B–V)_{tot} = 0.067$. Following the conversions from reddening

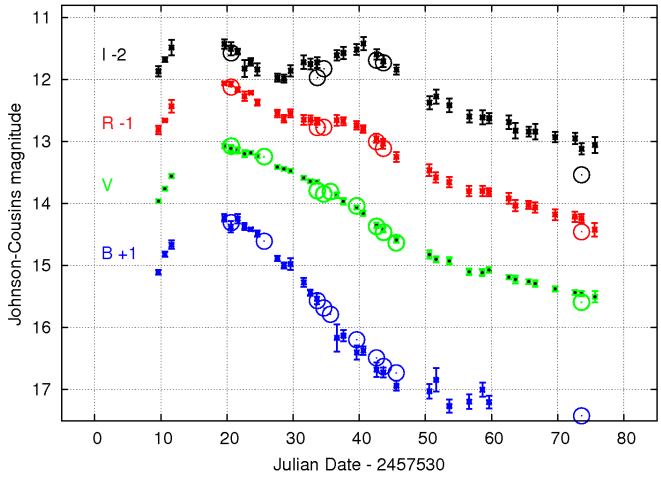

Figure 5. Light curves of SN 2016coj in BVRI. The data for each passband have been offset vertically for clarity. Small symbols represent measurements from RIT, large symbols those from NSO; uncertainties in the latter are smaller than the symbols.

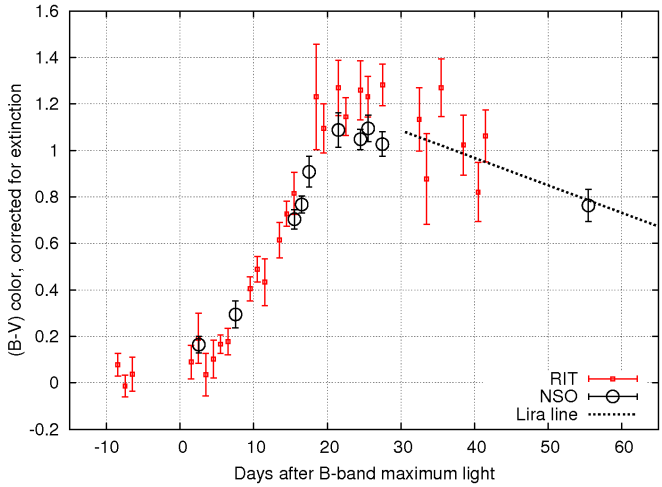

Figure 6. (B–V) color evolution of SN 2016coj, after correcting for extinction.

to extinction given in Schlafly and Finkbeiner (2011), we derive the extinction to SN 2016coj to be $A_B = 0.24$, $A_V = 0.18$, $A_R = 0.15$, and $A_I = 0.10$.

After removing this extinction from each passband, we calculate the evolution of the event in each color; see Figure 6 for (*B–V*), Figure 7 for (*V–R*), and Figure 8 for (*R–I*). The (*B–V*) color shows a value of zero at maximum light, typical for a normal type Ia. In the same figure, we have drawn a line which

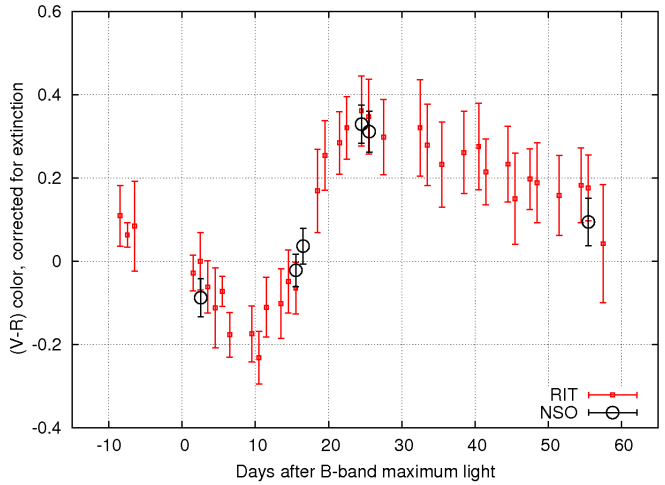

Figure 7. (V–R) color evolution of SN 2016coj, after correcting for extinction.

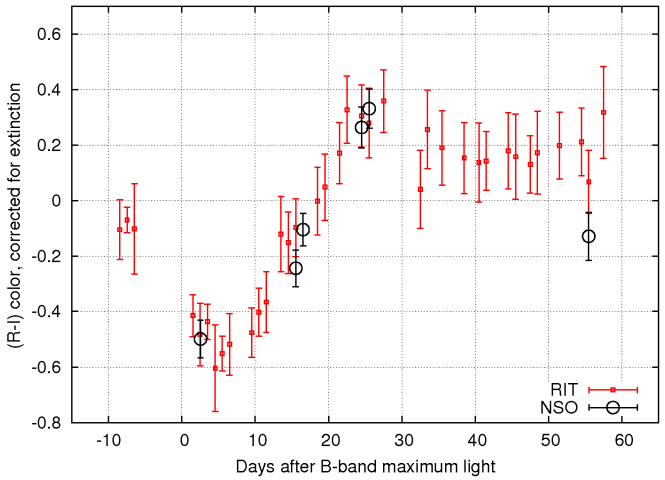

Figure 8. (R–I) color evolution of SN 2016coj, after correcting for extinction.

represents the late-time (*B*–*V*) evolution of a set of normal type Ia SNe with little or no extinction (Lira 1995; Phillips *et al.* 1999). Although our measurements are sparse and noisy at late times, due to the low signal in the *B* band, they suggest that SN 2016coj followed the same evolution as other normal events. In Figure 7, we see that SN 2016coj reaches a minimum (*V*–*R*) color about 10 days after *B*-band maximum, then increases to a maximum (*V*–*R*) = 0.35. The time of minimum is a few days earlier in (*R*–*I*), which then rises to a maximum of (*R*–*I*) = 0.35. All these properties are similar to those in the color curves of the normal SNe Ia 1994D (Richmond *et al.* 1995), 2003du (Stanishev *et al.* 2007), 2009an (Sahu *et al.* 2013), and 2011fe (Richmond and Smith 2012). The only significant difference in the late-time behavior of SN 2016coj is in (*R*–*I*), which appears to have a relatively constant value of (*R*–*I*) ~ 0.2. However, we believe that this color in particular suffers from a systematic bias in the RIT *I*-band measurements (see the Appendix); note the position of the single late-time NSO datum, at a negative color more typical of normal SNe.

5. Absolute magnitudes

What was the absolute magnitude of SN 2016coj? In order to convert our apparent magnitudes to the absolute scale, we need to account for extinction and the distance to the host galaxy (Table 5). As mentioned earlier, Zheng *et al.* (2016) place only upper limits on the extinction due to material in the host galaxy. In the discussion which follows, we will compute two values of absolute magnitude, one assuming no extinction in the host galaxy, the other corresponding to the upper limit of $E(B–V) = 0.05$ derived in Zheng *et al.* (2016). The distance to NGC 4125 has been measured a number of times, but none are very recent. We will adopt the measurement based on Surface Brightness Fluctuations (SBF) by Tonry *et al.* (2001) of $(m – M) = 31.89 \pm 0.25$.

Table 5. Absolute magnitudes of SN 2016coj at maximum light, corrected for extinction.

Passband	*E (B − V) = 0 in host*	*E (B − V) = 0.05 in host*	*based on* $\Delta m_{15}(B)$[a]
B	−18.79 ± 0.26	−18.97 ± 0.26	−19.19 ± 0.10
V	−18.88 ± 0.26	−19.01 ± 0.26	−19.12 ± 0.09
R	−18.89 ± 0.26	−18.99 ± 0.26	−19.14 ± 0.07
I	−18.68 ± 0.27	−18.76 ± 0.27	−18.87 ± 0.08
I (sec)	−18.41 ± 0.26	−18.49 ± 0.26	—

a. Using the relationship from Prieto et al. (2006).

A connection between the absolute magnitude of a type Ia SN and its rate of decline after maximum was first noted by Phillips (1993) and has since been refined by a number of authors (Hamuy *et al.* 1996; Riess *et al.* 1996; Perlmutter *et al.* 1997). We choose the relationships derived by Prieto *et al.* (2006) which are based on the fading in *B*-band in the first 15 days after maximum light, the $\Delta m_{15}(B)$ parameter. In the case of SN 2016coj, we measure $\Delta m_{15}(B) = 1.32 \pm 0.10$. Inserting that into the equations in Table 3 of Prieto *et al.* (2006) for events in environments with low extinction, we derive the absolute magnitudes shown in the rightmost column of Table 3. With the exception of the *B*-band measurement assuming no host extinction, all measurements agree with the predictions of the decline-rate method, supporting further the classification of SN 2016coj as normal. The slight improvement offered by assuming a small host extinction provides weak evidence that it may be close to the upper limits derived by Zheng *et al.* (2016).

6. Conclusion

Our measurements of SN 2016coj show that its photometric behavior at early times (within 60 days of maximum light) follows that of "normal" type Ia SNe. We compute a decline parameter of $\Delta m_{15}(B) = 1.32 \pm 0.10$ magnitude, placing it in the middle of the distribution of normal events. Adopting a distance modulus to NGC 4125 of $(m – M) = 31.89$ and correcting for a total of $E(B–V) = 0.067$ of extinction, we derive absolute magnitudes of $M_B = –19.01$, $M_V = –19.05$, $M_R = –19.03$, and $M_I = –18.79$.

We have shown that correcting for contamination of SN measurements by the background light of the host galaxy is a difficult issue for this event. While our measurements at early times—upon which the above conclusions are based—are reliable, those at late times must be treated with caution. The simple procedure we used for this dataset does not require

template images of the host galaxy alone, but can leave a systematic error which grows as the target object fades.

7. Acknowledgements

We thank the staff at AAVSO for their finding charts, sequences of comparison stars, and endless support of observers. MWR is grateful for the continued support of the RIT Observatory by RIT and its College of Science. BV thanks the Northeast Kingdom Astronomy Foundation for allowing him to use their facility. The Lick Observatory Supernova Search noticed this event and quickly alerted the rest of the community, permitting us to begin our study while the supernova was still on the rise. This research has made use of the "Aladin Sky Atlas" and SIMBAD database (Wenger *et al.* 2000), developed and operated at the CDS, Strasbourg Observatory, France, We have also made use of the NASA/IPAC Extragalactic Database (NED) which is operated by the Jet Propulsion Laboratory, California Institute of Technology, under contract with the National Aeronautics and Space Administration. This paper (and many others) has made use of NASA's Astrophysics Data System. Facility: AAVSO.

References

Chandrasekhar, S. 1931, *Astrophys. J.*, **74**, 81.

de Vaucouleurs, G., de Vaucouleurs, A., Corwin, H. G., Jr., Buta, R. J., Paturel, G., and Fouqué, P. 1991, *Third Reference Catalog of Bright Galaxies*, Springer, New York.

Diffraction Limited. 2012, MAXIMDL image processing software (http://www.cyanogen.com).

Filippenko, A. V., Li, W. D., Treffers, R. R., and Modjaz, M. 2001, in *Small Telescope Astronomy on Global Scales*, eds. B. Paczynski, W.-P. Chen, and C. Lemme, ASP Conf. Ser. 246, Astronomical Society of the Pacific, San Francisco, 121.

Guy, J., Astier, P., Nobili, S., Regnault, N., and Pain, R. 2005, *Astron. Astrophys.*, **443**, 781.

Hamuy, M., Phillips, M. M., Maza, J., Wischnjewsky, M., Uomoto, A., Landolt, A. U., and Khatwani, R. 1991, *Astron. J.*, **102**, 208.

Hamuy, M., Phillips, M. M., Suntzeff, N. B., Schommer, R. A., Maza, J., and Aviles, R. 1996, *Astron. J.*, **112**, 2391.

Landolt, A. U. 1992, *Astron. J.*, **104**, 340.

Leaman, J., Li, W., Chornock, R., and Filippenko, A. V. 2011, *Mon. Not. Roy. Astron. Soc.*, **412**, 1419.

Lira, P. 1995, Master's thesis, Univ. Chile.

Parrent, J. T., *et al.* 2012, *Astrophys. J., Lett.*, **752**, L26.

Perlmutter, S., *et al.* 1997, *Astrophys. J.*, **483**, 565.

Phillips, M. M. 1993, *Astrophys. J., Lett.*, **413**, L105.

Phillips, M. M., Lira, P., Suntzeff, N. B., Schommer, R. A., Hamuy, M., and Maza, J. 1999, *Astron. J.*, **118**, 1776.

Prieto, J. L., Rest, A., and Suntzeff, N. B. 2006, *Astrophys. J.*, **647**, 501.

Richmond, M. W., *et al.* 1995, *Astron. J.*, **109**, 2121.

Richmond, M. W., and Smith, H. A. 2012, *J. Amer. Assoc. Var. Star Obs.*, **40**, 872.

Riess, A. G., Press, W. H., and Kirshner, R. P. 1996, *Astrophys. J.*, **473**, 88.

Sahu, D. K., Anupama, G. C., and Anto, P. 2013, *Mon. Not. Roy. Astron. Soc.*, **430**, 869.

Schlafly, E. F., and Finkbeiner, D. P. 2011, *Astrophys. J.*, **737**, 103.

Schlegel, D. J., Finkbeiner, D. P., and Davis, M. 1998, *Astrophys J.*, **500**, 525.

Stanishev, V. *et al.* 2007, *Astron. Astrophys.*, **469**, 645.

Tonry, J. L., Dressler, A., Blakeslee, J. P., Ajhar, E. A., Fletcher, A. B., Luppino, G. A., Metzger, M. R., and Moore, C. B. 2001, *Astrophys. J.*, **546**, 681.

Treffers, R. R., and Richmond, M. W. 1989, *Publ. Astron. Soc. Pacific*, **101**, 725.

Wells, L. A., *et al.* 1994, *Astron. J.*, **108**, 2233.

Wenger, M., *et al.* 2000, *Astron. Astrophys., Suppl. Ser.*, **143**, 9.

Zheng, W., Yuk, H., Manzano-King, C., Canalizo, G., Sexton, R., Barth, A., Shivvers, I., and Filippenko, A. V. 2016, *Astron. Telegram*, No. 9095, 1.

Appendix: Bias in photometry

The location of SN 2016coj in its host galaxy presents the observer with good news and bad news. The good news is that NGC 4125 is an elliptical galaxy, and therefore likely contains relatively little gas and dust, as the spectroscopic measurements of Zheng *et al.* (2016) confirm. It is therefore not necessary to make large corrections for extinction. But the bad news is that the supernova is close enough to the bright core of its host, offset by only 5.0" east and 10.8" north (Zheng *et al.* 2016), that the light of the nucleus and the surrounding stars provides a significant background to measurements of the SN. Moreover, at this location, the light of the galaxy has a strong radial gradient, making it very difficult to subtract its contribution accurately.

Since other observers may encounter similar situations, we describe in some detail below our investigation of the likely systematic errors that can arise when one attempts to perform photometry on such images.

It became clear to us that simple aperture photometry methods would yield poor results in this case. Since we did not have template images of the galaxy to use as references for subtraction in the standard manner, we settled upon a method which would provide better (but not perfect) results: making a copy of each image, rotating the copy by 180° around the center of the galaxy, then subtracting the copy from the original. As shown in Figure 2, the resulting residual image has a background near the location of the supernova which is both much lower, and much more uniform, than the original image. We used these residual images to derive the measurements presented in this paper.

However, we suspected that there remained a sometimes significant systematic error in the photometry produced by this method, for two reasons. First, when comparing the decline of SN 2016coj against that of other type Ia SNe, such as SN 2011fe, we noticed that this event faded less quickly at late times—by an amount which appeared to grow with time. Second, we noticed a difference between measurements from our two sites: measurements from NSO, which typically have a smaller PSF and higher signal-to-noise than those from RIT, showed the SN as slightly fainter, and this difference also grew with time.

Could there be a reason why measurements of faint point sources immersed in a noisy (and possibly non-uniform) background should show a systematic error? Our technique of identifying and measuring both reference stars and the supernova in images was a simple one: we searched through each image independently to identify peaks above the local sky background, measured their properties, and kept as "good" sources those which had shapes consistent with the expected PSF. We used the pixels around each of these sources to compute its center, placed a circular aperture at this position, and integrated the light within the aperture; finally, we subtracted the contribution from the local background light within the aperture.

The important feature of this standard method is that the position of the aperture used to measure the SN (and reference stars) is not fixed in any way: it may be influenced independently by noise in each image, especially when the source is faint and the noise is high. A better technique, one which is natural when using a template, is to align images, co-add them to improve signal-to-noise, and measure relative positions for the SN and several reference stars; then, in each individual image, measure the position of bright reference stars and use them to *infer* the position of the SN using a fixed offset, rather than computing it based on the possibly noisy data at its location in each image. The method we employed is likely to shift the center of the SN's aperture slightly to follow positive noise peaks, which could yield measurements slightly higher than they ought to be.

In short, we suspect that our measurements, especially those made at RIT, contain a systematic positive bias: the SN appears brighter than it actually is, by an amount which increases as the SN fades.

To test this hypothesis, we created a set of simulated images with properties similar to those acquired at RIT, and subjected them to exactly the same measurement methods as we used on our actual images. We started with a simplified situation: a set of reference stars of identical brightness on a uniform background, and a single "supernova" immersed in a "square galaxy" region of uniform higher intensity; see Figure 9. The stars are modeled as gaussians of FWHM 3.0 pixels, matching the typical seeing at RIT, and the gain in the image is set to 2.2 electrons per count, matching the properties of the SBIG ST-9E camera. The brightness of the "square galaxy" is set to 620 counts, typical for the region near SN 2016coj in *R*-band images. Note that the stars are placed at intervals with small random variations, ensuring that they appear at a wide range of sub-pixel locations. We ran a number of instances of each simulation, shifting both the reference stars and the "supernova" by small random sub-pixel positions each time.

In this simplified situation, we chose as the center of rotation the geometric center of the image. After making a copy and rotating it around this center by 180°, we subtracted the copy from the original, leaving both reference stars and "supernova" in a near-zero background; but the pixels surrounding the supernova might be noisier than those surrounding the reference stars. As a sanity check that our software was not introducing errors of its own, we ran simulations in which no photon noise was added to the images: the background value was some fixed value in all pixels, and the model gaussian for each star was similarly exact. Over a series of trials, the reference stars and "supernova" were all set to the same input brightness, increasing gradually throughout the trials until their centers reached a value of 30,000 counts (similar to the limit of linearity on our camera). We would expect the stars and "supernova" all to have exactly the same magnitude in this noiseless simulation. The magenta symbols in Figure 10 show that the difference between the average reference star magnitude, and the "supernova" magnitude, is indeed zero under these conditions.

However, when we add photon noise to our simulations, we find some differences between the magnitude of the reference stars and the "supernova." We ran simulations with two background levels, 100 and 1,000 counts per pixel, roughly bracketing the range of sky levels in real RIT images (which varies due to clouds, haze, and the aspect of the Moon). Consider first the red asterisk symbols, which show the results under low sky conditions: when the SN and stars are bright, there is no significant difference in their measured magnitudes. But when the stars are faint, noise in the sky background and in their own signal leads both to increased scatter and to discrepancy between the average value of the reference stars and that of the "supernova"; the SN tends to be measured as brighter than the reference stars. The amplitude of the difference grows to roughly 0.1 magnitude by the time the stars are too faint to detect reliably. The blue circular symbols, corresponding to higher and so noisier background sky levels, show the same trend, but at an increased amplitude.

We conclude that point sources simply immersed in a higher background of light will suffer from a systematic bias under our measurement procedure, appearing brighter than they ought to be. However, the situation of SN 2016coj is even worse: not only is it in a region of higher background level than the comparison stars, but it sits in a strong spatial gradient. What effect will this additional complication have on our measurements?

We performed a very simple test by creating a toy model of our real images. We created an artificial galaxy by superposing a central gaussian (FWHM = 3.0 pixels) and an extended and flattened component (FWHM = 8.0 pixels, convolved with a kernel of FWHM = 6 along rows and FWHM = 12 along columns), scaling the result so that it resembled the appearance of NGC 4125 in our *R*-band images. We then placed the "supernova" at an offset from the galaxy similar to its actual offset. Both the galaxy and the "supernova" were shifted in position by small random sub-pixel amounts in each realization of our simulations. Figure 11 shows an example of these artificial images, one in which the reference stars and SN are all at the maximum brightness.

We then carried out a series of instances, changing the brightness of the stellar objects over a wide range; at each level of brightness, we ran ten realizations, varying the positions of each source at the sub-pixel level and generating different random values of photon noise. For each realization, we carried out exactly the same measurement procedure as we used for the real images:

- a copy of the image was displayed on a computer screen
- the user moved a cursor to the center of the galaxy, pressed

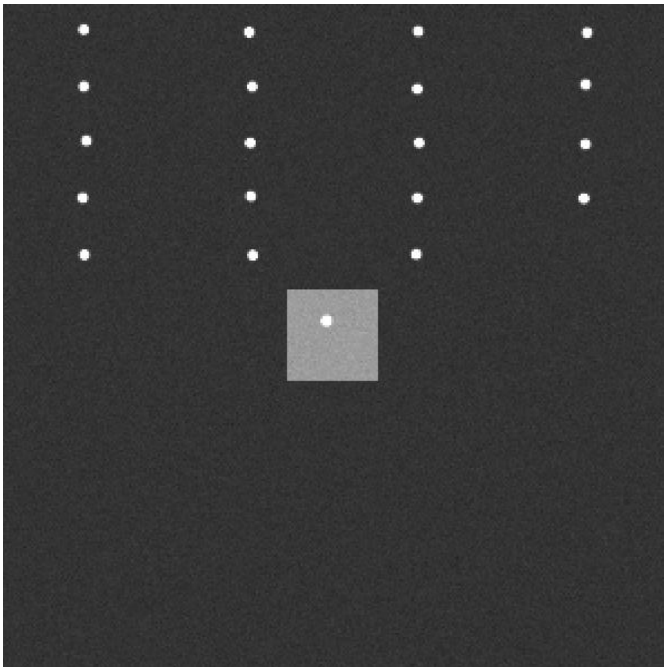

Figure 9. Simulated image with 19 reference stars in a low background and a "supernova" immersed in a "square galaxy."

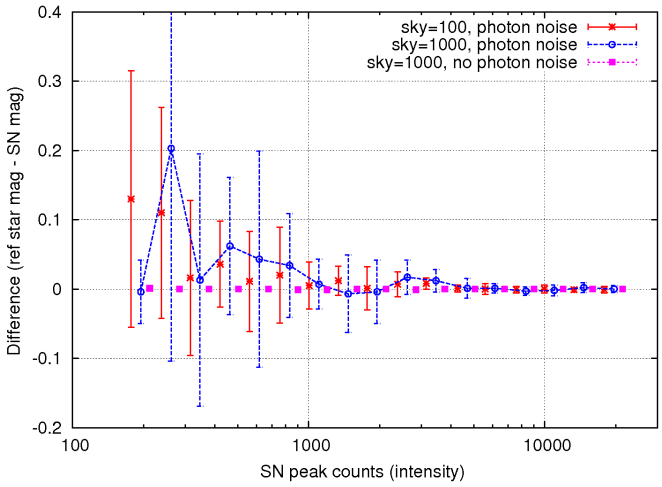

Figure 10. Results of photometry after rotation and subtraction of the simulated images with a "square galaxy."

a key to initiate a calculation of the local centroid and display a radial profile, made adjustments to initial position until satisfied that the center had been found correctly

• a copy of the image was rotated around this position

• the copy was subtracted from the original image

• point sources in the residual image were automatically found and measured via aperture photometry

An example of one residual image is shown in Figure 12. There is clearly imperfect subtraction of the galaxy's light at its very center, as is seen in most of the real images after this procedure.

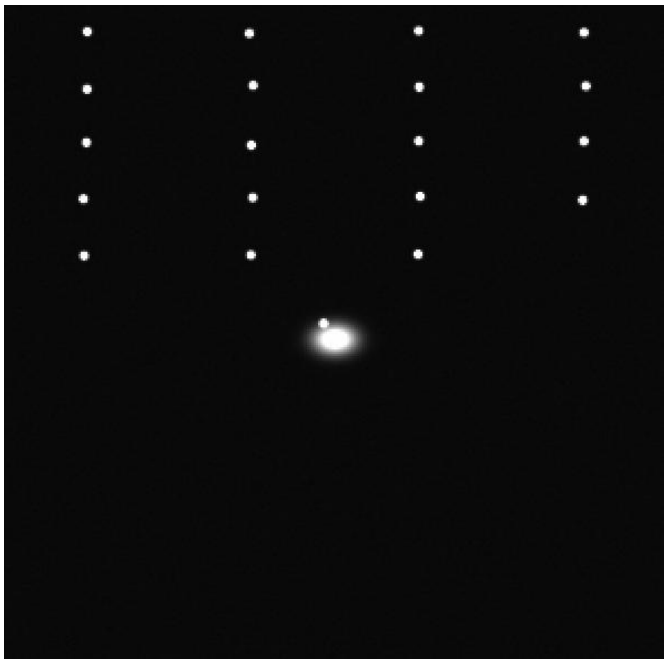

Figure 11. Simulated image with 19 reference stars in a low background and a "supernova" placed close to an artificial galaxy.

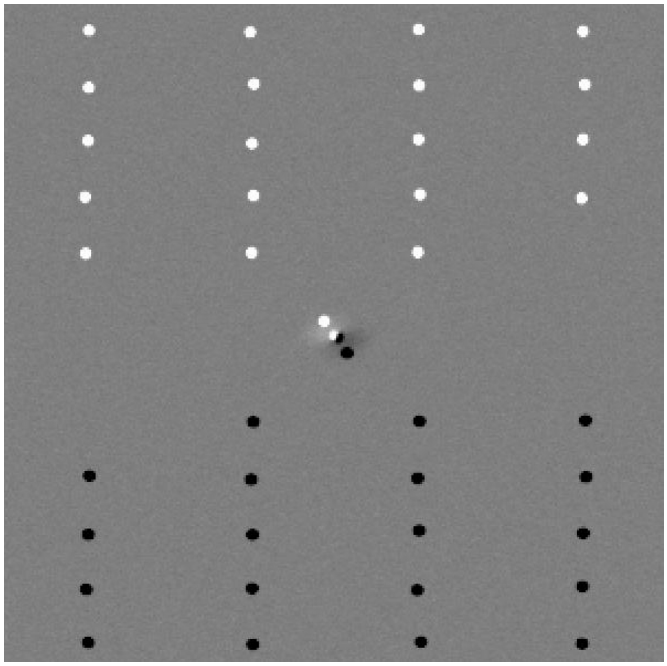

Figure 12. Simulated image with artificial galaxy after rotation and subtraction.

The results of photometry on these images are display in Figure 13. In this case, we fixed the brightness of the overall sky background to 100 counts for all realizations, so it represents the optimistic end of the spectrum of real conditions. The general trend is similar to that in the "square galaxy" simulations: measurements of the SN appear brighter than those of the reference stars, by an amount which increases as the SN fades. However, there are important differences: first, this systematic difference appears even in the absence of photon noise; this indicates that the software used to perform the image analysis

(XVISTA; Treffers and Richmond 1989) is unable to compute the center of the galaxy accurately enough, or perform the image rotation accurately enough, or both. Second, note that the *amplitude* of the systematic difference is much larger than in the "square galaxy" simulations: the SN can appear about 1.0 magnitude brighter it ought to be, instead of just 0.1 magnitude.

In order to reduce these systematic errors, one must improve the method of subtracting the background contribution to the total light within the photometric aperture. Given the large FWHM of our images, we could not decrease the size of the photometric aperture significantly; given the location of the SN, close to the galaxy's nucleus, increasing the size of the background annulus would make matters worse, and, given the large FWHM, decreasing the size of the background annulus is not possible. Rather than choosing some constant value per pixel for the background contribution, one could do better by making a model of the galaxy's light within the photometric aperture. We will investigate this technique in the future; it would require a substantial effort to modify the existing software. The difficulty of proper background subtraction is, of course, the reason that many astronomers adopt the "template subtraction" method.

Now, in light of this information, let us review the light curves shown in Figure 5. When the SN is bright, measurements from RIT and NSO agree well; but as the SN fades, an offset between the two datasets appears, with the NSO measurements slightly fainter. The offset is largest in the *I*-band and smallest in the *B*-band; we ascribe this trend with wavelength to the color of the galaxy's light. The starlight of NGC 4125 is more prominent at long wavelengths, making the background at the location of

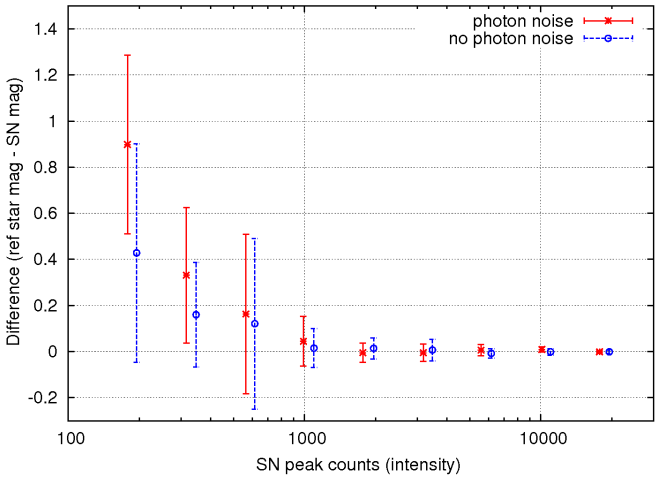

Figure 13. Results of photometry after rotation and subtraction of the simulated images with a realistic galaxy model.

SN 2016coj brightest (relative to the SN) in the *I*-band. Since the NSO data have both a smaller PSF and a higher signal-to-noise ratio, they suffer from less contamination by the galaxy's light.

At early times, the SN was bright enough that any systematic bias was at most comparable to the random uncertainties in each measurement; but that is certainly not true for the late times. We recommend that readers use with caution the latest measurements presented here. We suggest that greater weight be given to the NSO values at late times; it might be profitable to "warp" the RIT measurements at late times to match the final NSO magnitudes.